Supporting Information:

Molecular Interactions of Photosystem 1 and ZIF-8 in Bio-Nanohybrid Materials

Sebastian Reiter,[*,†] Igor Gordiy,[†] Kathrin L. Kollmannsberger,[‡] Feng Liu,[¶] Erling Thyrhaug,[§] Dario Leister,[¶] Julien Warnan,[‡] Jürgen Hauer,[*,§] and Regina de Vivie-Riedle[†]

[†]*Department of Chemistry, Ludwig-Maximilians-Universität München, Butenandtstr. 11, 81377 Munich, Germany*

[‡]*Chair of Inorganic and Metal-Organic Chemistry, Department of Chemistry and Catalysis Research Center (CRC), TUM School of Natural Sciences, Technical University of Munich, Lichtenbergstr. 4, 85748 Garching, Germany.*

[¶]*Faculty of Biology, Ludwig-Maximilians-Universität München, Großhaderner Str. 2-4, 82152 Planegg-Martinsried, Germany.*

[§]*Professorship of Dynamic Spectroscopy, Department of Chemistry and Catalysis Research Center (CRC), TUM School of Natural Sciences, Technical University of Munich, Lichtenbergstr. 4, 85748 Garching, Germany.*

E-mail: sebastian.reiter@cup.uni-muenchen.de; juergen.hauer@tum.de

Contents

1 Gromacs Port of nb-ZIF-FF

nb-ZIF-FF models the interactions between the ZIF-8 building blocks as non-bonded interactions between dummy atoms (fig. S1). The general form of the force field is given by eq. (1). For bonds, k_b describes the bond stretching constant, b the bond length and b_0 the equilibrium bond length. Valence angles are described by the sum of a harmonic potential and a Urey-Bradley term, where k_θ is the harmonic force constant, θ is the angle and θ_0 denotes the equilibrium angle. Analogously, k_{UB} denotes the Urey-Bradley force constant, r the 1–3 distance and r_0 the equilibrium 1–3 distance. Dihedral angles are modelled by periodic cosine potentials, where k_ϕ is the force constant, ϕ is the dihedral, n is the frequency of the cosine and, in the case of torsions, d denotes the phase. Non-bonded dispersive interactions are described by Lennard-Jones (LJ) 12–6 potentials, where σ_{ij} is the distance at which the two-particle potential is zero, ϵ_{ij} is the dispersion energy and r_{ij} is the distance between two particles. Electrostatic interactions are described by Coulomb potentials, where q_i and q_j are the partial charges of the interacting particles and ε_0 denotes the electric field constant.

$$
\begin{aligned}
E = &\sum_{bonds} k_b(b - b_0)^2 + \\
&\sum_{angles} k_\theta(\theta - \theta_0)^2 + k_{UB}(r - r_0)^2 + \\
&\sum_{torsions} k_\phi[1 + \cos(n\phi - d)] + \\
&\sum_{impropers} k_\phi[1 - \cos(n\phi)] + \\
&\sum_{i}^{N} \sum_{j=i+1}^{N} \left(4\epsilon_{ij} \left[\left(\frac{\sigma_{ij}}{r_{ij}} \right)^{12} - \left(\frac{\sigma_{ij}}{r_{ij}} \right)^{6} \right] + \frac{q_i q_j}{4\pi\varepsilon_0 r_{ij}} \right)
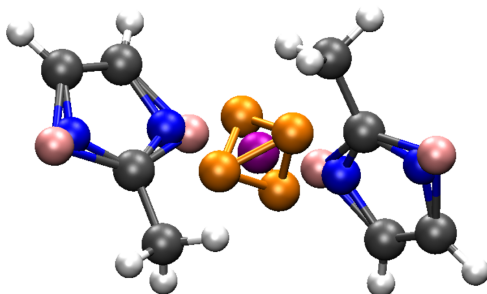\end{aligned}
\tag{1}
$$

Figure S1: Scheme of the cationic and anionic dummy-atom models for Zn^{2+} and MIm^- (gray: C, blue: N, white: H, purple: Zn, orange: Zn dummy atoms, pink: N dummy atoms).[S1]

The original implementation of nb-ZIF-FF is published for use with *LAMMPS*,[S1,S2] but the calculations in the present work were conducted with *Gromacs*, which uses a different system of units. Therefore, the force constants were converted using the conversion factors provided in table S1. The ported force field parameter files are openly available at

https://doi.org/10.5281/zenodo.12546403

Table S1: Conversion factors used to convert the nb-ZIF-FF force-field parameters from LAMMPS format (source file `forcefield.lmp`) into GROMACS format. The units were converted by multiplication with the corresponding conversion factor. The same conversion factor was used for both dihedrals and improper dihedrals.

Type	Parameter	Factor	LAMMPS	Gromacs
Bonded	b_0	0.1	Å	nm
	r_{13}	0.1	Å	nm
	k_b	836.8	$0.5\,\mathrm{kcal\,mol^{-1}\,Å^{-2}}$	$\mathrm{kJ\,mol^{-1}\,nm^{-2}}$
	k_{UB}	836.8	$0.5\,\mathrm{kcal\,mol^{-1}\,Å^{-2}}$	$\mathrm{kJ\,mol^{-1}\,nm^{-2}}$
	k_θ	8.368	$0.5\,\mathrm{kcal\,mol^{-1}\,rad^{-2}}$	$\mathrm{kJ\,mol^{-1}\,rad^{-2}}$
	k_ϕ	4.184	$\mathrm{kcal\,mol^{-1}}$	$\mathrm{kJ\,mol^{-1}}$
Non-bonded	σ	0.1	Å	nm
	ϵ	96.4869	eV	$\mathrm{kJ\,mol^{-1}}$

In the original implementation, the interactions between Zn^{2+} and MIm^- are modelled by a Morse potential, which is not available in *Gromacs*. Simple application of the Lorentz-Berthelot mixing rules to the σ_{ij} and ϵ_{ij} parameters of the two atom types does not fit the original Morse potential well (fig. S2). Therefore, a custom 12–6-LJ potential was fitted to describe the Zn^{2+}/MIm^- interaction, resulting in the following parameters:

$$\sigma_{ij} = 0.2442\,\mathrm{nm}$$
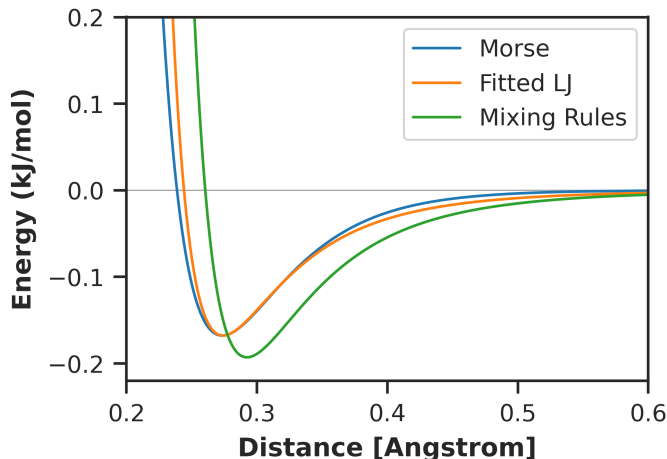$$\epsilon_{ij} = 0.1678\,\mathrm{kJ\,mol^{-1}}.$$

Figure S2: Fit of the non-bonded interactions between Zn^{2+} and MIm^- in nb-ZIF-FF with a LJ potential. For comparison, the LJ potential resulting from application of the Lorentz-Berthelot mixing rules to the original σ and ϵ parameters is also shown.

Moreover, 1–4 Coulomb interactions are scaled by a factor of 0.6874 in the original force field.[S1] However, the PS I model[S3] employs a scaling factor of 0.8333, compatible with the Amber force field. As the main interest of this work is in the photosystem we retained and used the factor of 0.8333 in all simulations.

To validate the ported force field, we performed a series of MD simulations on ZIF-8 in various environments and compared the results to the original work.[S1] All of these control simulations were conducted with the leap-frog integrator, using a time step of 0.5 fs and constraining bonds to hydrogen atoms with the LINCS algorithm.[S4] Short-range interactions were evaluated with Verlet lists,[S5] using a cutoff of 1.4 nm (in methanol) or 1.2 nm (in water), while the smooth particle-mesh Ewald scheme[S6,S7] was used for long-range interactions with a Fourier grid spacing of 0.16 nm and fourth-order interpolation.

In analogy to the reference work,[S1] we first set up a solution of the ZIF-8 building blocks in methanol, describing the solvent with the TraPPE force field.[S8] The cubic simulation box had an edge length of 4.6 nm and contained 125 Zn^{2+} ions, 250 MIm^- ions and 825 methanol molecules. The energy of the system was minimized until the maximum force was below $1000\,\mathrm{kJ\,mol^{-1}\,nm^{-1}}$ and the system was equilibrated in two phases: First, the temperature was annealed from 10 K to 300 K over 1 ns and propagated for another 200 ps in an NVT ensemble controlled by the V-rescale thermostat[S9] using a time constant τ_T of 0.1 ps. Subsequently, the pressure was equilibrated to 1 bar in an NPT ensemble controlled by the Berendsen barostat,[S10] using a time constant τ_p of 2.5 ps and an isothermal compressibility of $6.02 \times 10^{-5}\,\mathrm{bar^{-1}}$ for methanol,[S11] while keeping the thermostat settings from the previous step. The production MD was conducted for 15 ns in the same NPT ensemble, while raising

the temperature from $300\,\mathrm{K}$ to the $400\,\mathrm{K}$ discussed in the reference work[S1] within the first $1.5\,\mathrm{ns}$. From fig. S3 it is obvious that the methanol solution of Zn^{2+} and MIm^- ions undergoes spontaneous self-assembly and forms an amorphous phase, just like with the original force field.[S1]
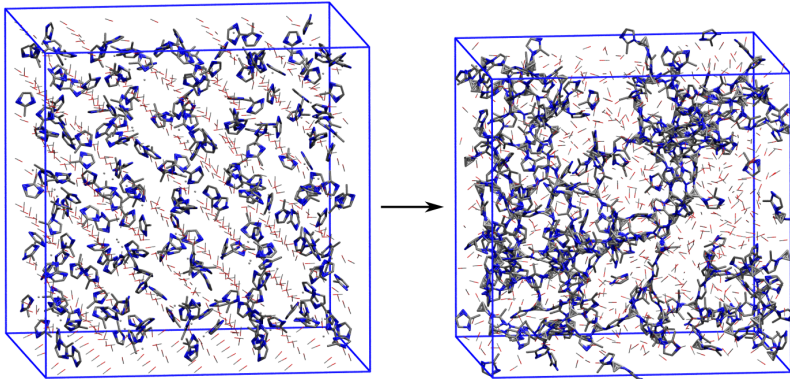

Figure S3: Control MD simulation of ZIF-8 building blocks in methanol. Starting from the initial configuration before equilibration (left), the building blocks undergo self-assembly to form an amorphous phase (right). H-atoms omitted for clarity.

Next, we set up two ZIF-8 crystals, solvated in methanol and in water, respectively. The cubic simulation boxes had an edge length of $3.63\,\mathrm{nm}$ (methanol) and $3.44\,\mathrm{nm}$ (water) after equilibration and contained 96 Zn^{2+} ions, 192 MIm^- ions and 379 (methanol) or 541 (water) solvent molecules. Both were equilibrated according to the same protocol: First, the energy was minimized until the maximum force was below $1000\,\mathrm{kJ\,mol}^{-1}\,\mathrm{nm}^{-1}$. Next, the temperature was raised from $10\,\mathrm{K}$ to $300\,\mathrm{K}$ over $2\,\mathrm{ns}$ in an NVT ensemble, controlled by the V-rescale thermostat[S9] ($\tau_T = 0.1\,\mathrm{ps}$). The system was propagated in the same ensemble at constant temperature for another $1\,\mathrm{ns}$. In the second step, the system was equilibrated for $2\,\mathrm{ns}$ in an NPT ensemble at $1\,\mathrm{bar}$, controlled by the Berendsen barostat[S10] ($\tau_p = 2.5\,\mathrm{ps}$). The isothermal compressibility was set to $6.02 \times 10^{-5}\,\mathrm{bar}^{-1}$ for methanol[S11] and $4.5 \times 10^{-5}\,\mathrm{bar}^{-1}$ for water.[S12] The temperature was kept stable at $300\,\mathrm{K}$ using the same settings as before. Production MD simulations were conducted for $1\,\mathrm{ns}$ in the same ensemble. The Zn^{2+}–Zn^{2+} radial distribution function (RDF) were evaluated in both simulations (fig. S4) and found to agree well with that of the original force field implementation[S1] and an experimentally determined[S13] RDF. For comparison, fig. S4 also depicts the RDF for the PS I@ZIF-8 simulation, which also agrees well with the reference.
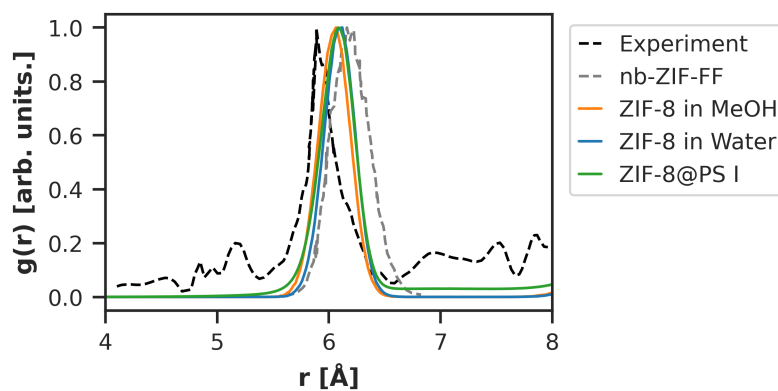
Figure S4: Normalized Zn^{2+}-Zn^{2+} radial distribution function in various control simulations compared to literature values.[S1,S13] Satellite peaks in the experimentally determined RDF are most likely due to defects in the crystal structure. The RDF from the present work is averaged over the entire trajectory and thus smoother than the calculated reference RDF.

2   Structural Changes of PS I in Water
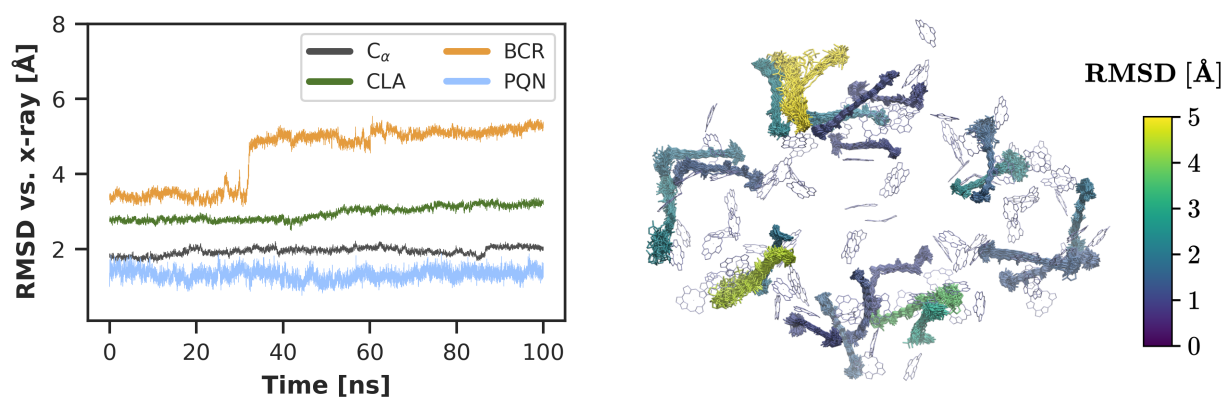
Figure S5: RMSD of key PS I components in water. C_α: Protein backbone, CLA: chlorophyll *a*, BCR: β-carotene, PQN: phylloquinone. The jump in the β-carotene RMSD at 32 ns is due to the reorientation of a peripheral carotenoid, as shown on the right, where the motion of the carotenoids over 100 ns is illustrated with respect to the first frame of the trajectory (view from the stromal side).

3 MD of PS I in Solution with MImH and MImH$_2^+$

To investigate the effects of the linker alone, without Zn^{2+} ions, we performed an MD simulation and investigated the coordination of the chlorophylls. To this end, the PS I model was placed in a triclinic box with dimensions $23 \times 23 \times 18$ nm and solvated by $297\,327$ water molecules. The pKa values of 2-methylimidazole are 7.7 (MImH$_2^+$/MImH) and 14.7 (MImH/MIm$^-$), so that the concentration of MIm$^-$ in a buffered solution around pH 9 is negligible. Thus, water molecules were randomly replaced by 4300 MImH molecules and 4300 MImH$_2^+$ ions.

Parameters for MImH and MImH$_2^+$ were generated with *antechamber*[S14] using the *GAFF2* force field.[S15] Charge neutralization was achieved by adding 4285 Cl$^-$ ions. The final system contained $900\,460$ atoms and was equilibrated using the same protocol as for the MD in amorphous ZIF-8, described in the main article. A production simulation was carried out for 100 ns. Even though the MImH$_2^+$ cation is over-represented in the simulation, it does expectedly not coordinate to the also positively charged chlorophyll centers. In contrast, the neutral MImH coordinates often to the Mg^{2+} ions of the peripheral chlorophylls in PS I (fig. S6). Neither MImH, nor MImH$_2^+$ induce a CT to the chlorophylls, as shown in sections 5.3 and 5.4.
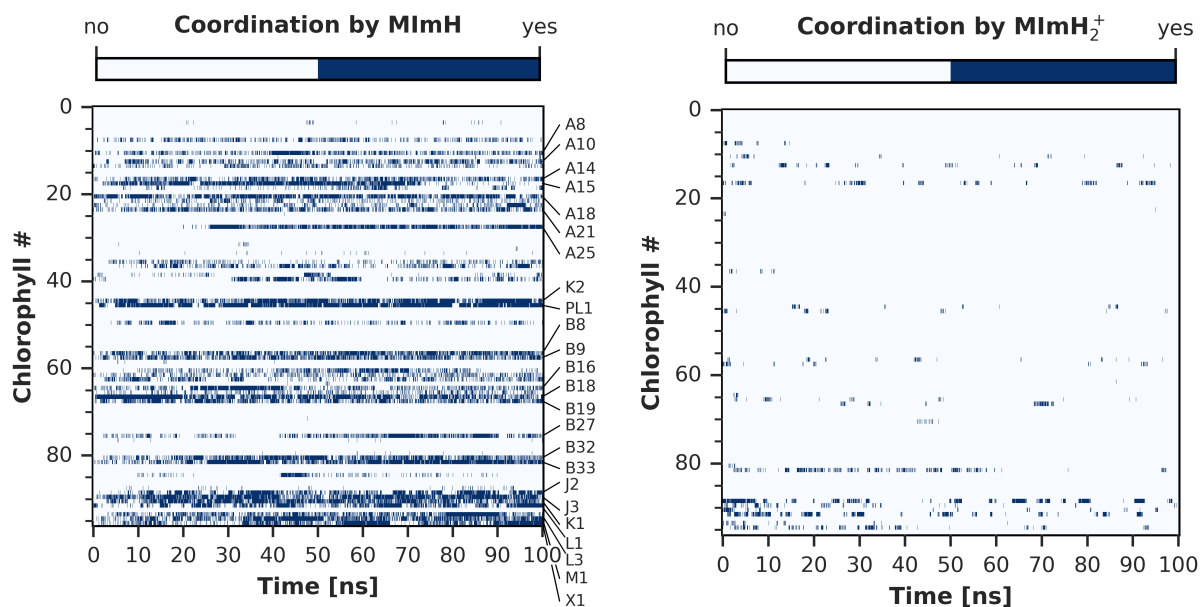
Figure S6: Coordination of chlorophylls by ZIF-8 building blocks at neutral pH. Coordination is defined as any ligand atom closer than 4.0 Å to the respective Mg^{2+} ion. Labels denote chlorophylls which are coordinated for more than 40 % of the trajectory.

4 Further Structural Analysis of PS I@ZIF-8
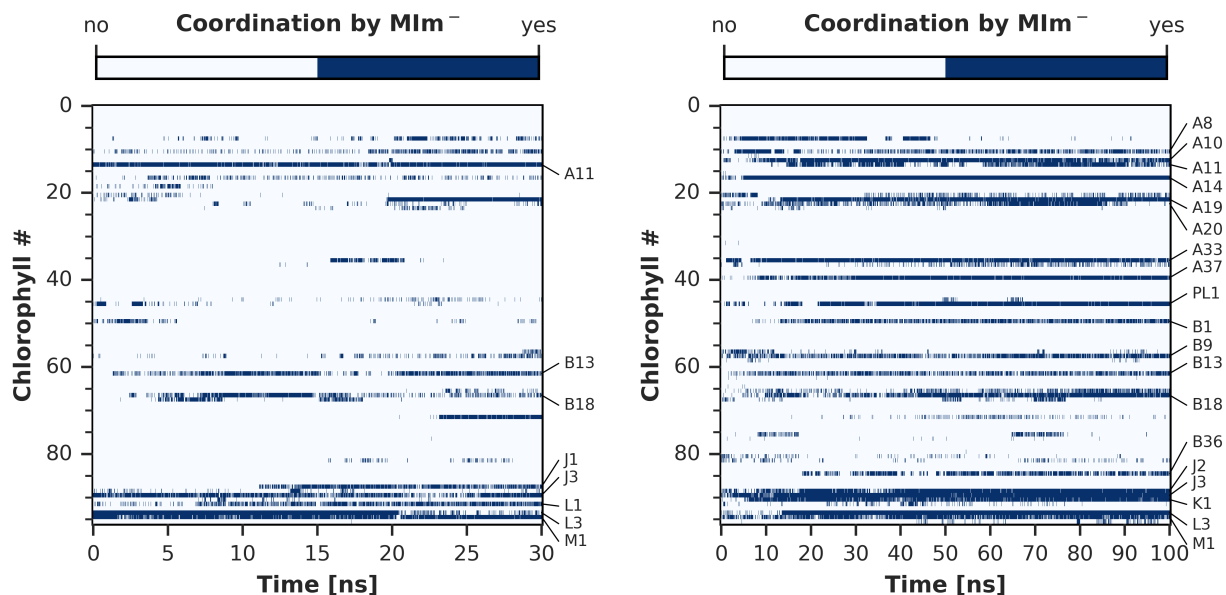
Figure S7: Coordination of chlorophylls by MIm⁻ residues over the course of the PS I@ZIF-8 trajectory inside the ZIF-8 crystal (left) and in amorphous ZIF-8 (right). Coordination is defined as any ligand atom closer than 4.0 Å to the respective Mg^{2+} ion. Labels denote chlorophylls which are coordinated for more than 40 % of the trajectory.
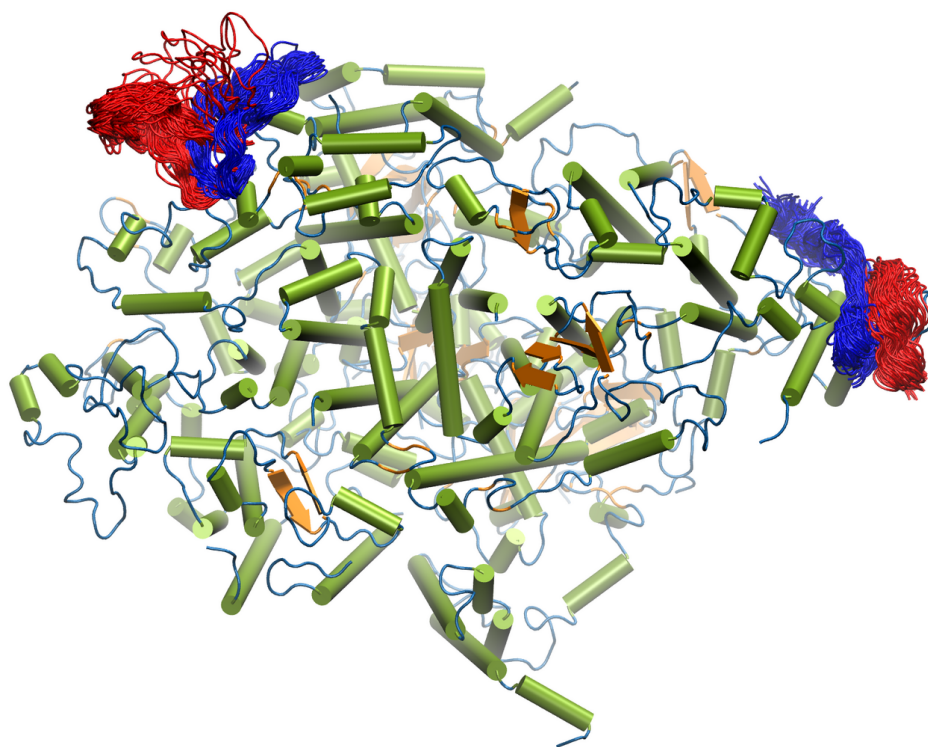
Figure S8: Difference in the N-terminal loop orientations of chain K (right) and F (top) over the course of the 100 ns trajectories of PS I in amorphous ZIF-8 (red) compared to PS I in water (blue). View from the lumenal side.
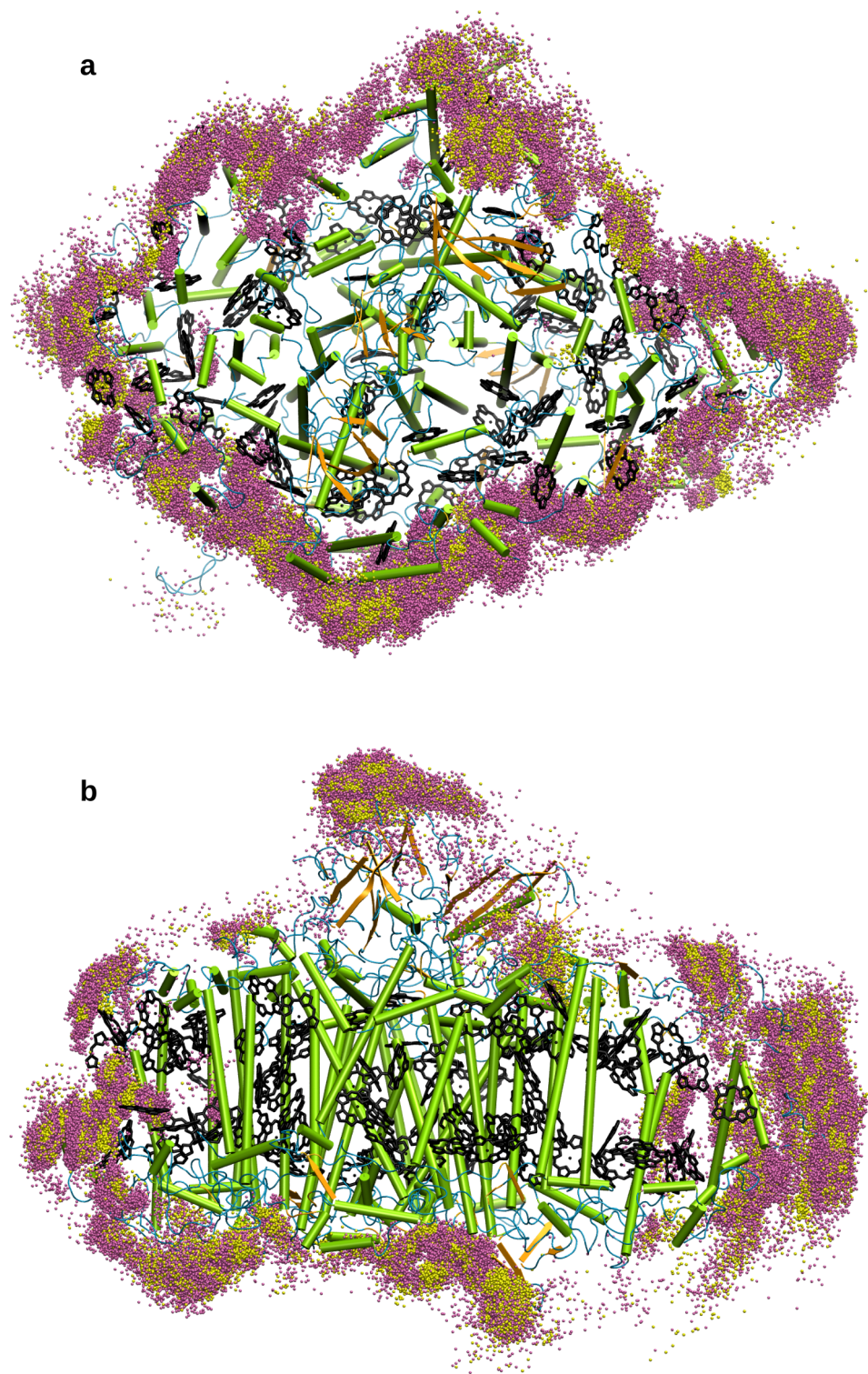
Figure S9: Permeation of the protein matrix by Zn^{2+} (magenta) and MIm^- (yellow) ions during the 100 ns trajectory of PS I in amorphous ZIF-8. Zn^{2+} and MIm^- positions are accumulated over all time steps in this illustration. (a) View from the stromal side and (b) rotated by 90° around x with respect to (a).

5 Excited States

5.1 Neutral and anionic chlorophyll *a*

Table S2: Isolated Chl *a*, DFT/MRCI. The respective orbitals are illustrated in fig. S10.

state	ΔE [eV]	osc	CI weight	CI transition
S_1	1.97	0.3495	0.731	$\pi_1 \to \pi_1^*$
S_2	2.22	0.0337	0.574	$\pi_2 \to \pi_1^*$
			0.247	$\pi_1 \to \pi_2^*$
S_3	3.07	0.0667	0.693	$\pi_3 \to \pi_1^*$
S_4	3.09	0.8657	0.490	$\pi_1 \to \pi_2^*$

Table S3: Isolated Chl *a*, SCS-ωPBEPP86/def2-TZVP. The respective orbitals are illustrated in fig. S10.

state	ΔE [eV]	osc	CI weight	CI transition
S_1	1.90	0.3018	0.765	$\pi_1 \to \pi_1^*$
S_2	2.17	0.0254	0.523	$\pi_2 \to \pi_1^*$
			0.395	$\pi_1 \to \pi_2^*$
S_3	3.23	0.4931	0.211	$\pi_1 \to \pi_2^*$
			0.400	$\pi_4 \to \pi_1^*$
S_4	3.33	1.3134	0.292	$\pi_1 \to \pi_2^*$
			0.232	$\pi_2 \to \pi_1^*$
			0.266	$\pi_4 \to \pi_1^*$
S_5	3.37	0.0335	0.595	$\pi_5 \to \pi_1^*$
S_6	3.39	1.3591	0.591	$\pi_2 \to \pi_2^*$
S_7	3.69	0.2950	0.587	$\pi_6 \to \pi_1^*$
S_8	3.71	0.0047	0.296	$LP_O \to \pi_1^*$
			0.335	$LP_O \to \pi_3^*$

Table S4: Isolated Chl a^-, DFT/MRCI. Note that the MO π_1^* is singly occupied and can serve as both a donor and acceptor orbital. The respective orbitals are illustrated in fig. S10.

state	ΔE [eV]	osc	CI weight	CI transition
S_1	0.80	0.0376	0.767	$\pi_1^* \to \pi_2^*$
S_2	1.49	0.0610	0.579	$\pi_1 \to \pi_1^*$
S_3	1.58	0.0475	0.701	$\pi_2 \to \pi_1^*$
S_4	1.81	0.2095	0.526	$\pi_1^* \to \pi_3^*$

Table S5: Isolated Chl a^-, SCS-ωPBEPP86/def2-TZVP. Note that the MO π_1^* is singly occupied and can serve as both a donor and acceptor orbital. The respective orbitals are illustrated in fig. S10.

state	ΔE [eV]	osc	CI weight	CI transition
S_1	1.26	0.0735	0.708	$\pi_1^* \to \pi_2^*$
S_2	1.69	0.0389	0.633	$\pi_1 \to \pi_1^*$
S_3	2.24	0.1089	0.277	$\pi_1 \to \pi_2^*$
			0.320	$\pi_2 \to \pi_1^*$
S_4	2.25	0.1011	0.464	$\pi_1^* \to \pi_3^*$
S_5	2.51	0.1402	0.292	$\pi_3 \to \pi_1^*$
S_6	2.57	0.0749	0.230	$\pi_2 \to \pi_1^*$
S_7	2.78	0.0057	0.215	$\pi_1^* \to \pi_4^*$
S_8	2.90	0.4448	0.220	$\pi_2 \to \pi_2^*$

Gouterman MOs
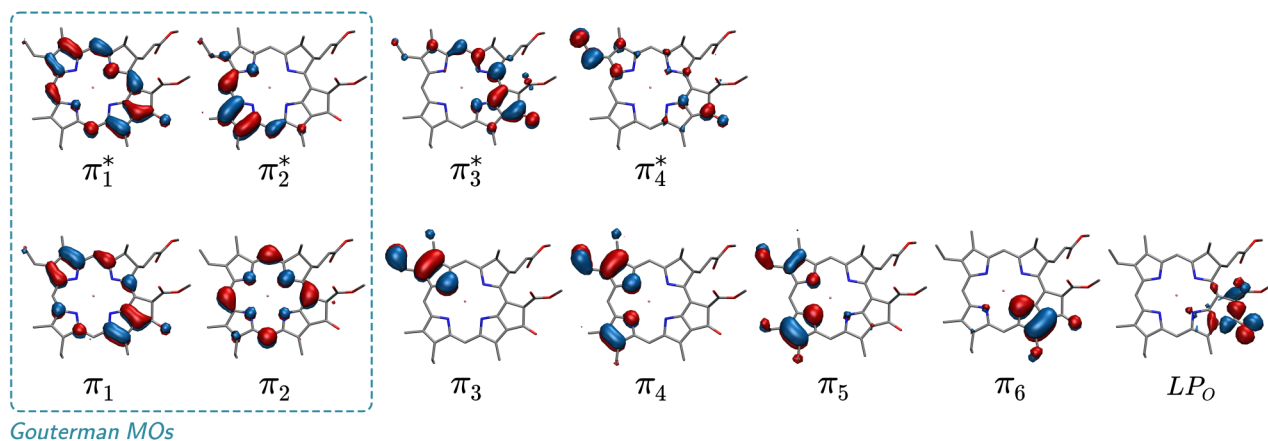
Figure S10: MOs with labels as in tables S2 to S5 (Isovalue: 0.02).

5.2 Chlorophyll $a \cdots$ MIm$^-$ assembly

Table S6: Chl $a \cdots$ MIm$^-$, Franck-Condon point, DFT/MRCI. The respective orbitals are illustrated in fig. S11.

state	ΔE [eV]	osc	CI weight	CI transition
S$_1$	1.94	0.2452	0.383	$\pi_1 \rightarrow \pi_1^*$
			0.370	$\pi_{\text{MIm}^-,1} \rightarrow \pi_1^*$
S$_2$	1.98	0.0900	0.497	$\pi_{\text{MIm}^-,1} \rightarrow \pi_1^*$
			0.329	$\pi_1 \rightarrow \pi_1^*$
S$_3$	2.10	0.0483	0.643	$\pi_2 \rightarrow \pi_1^*$
S$_4$	2.74	0.0153	0.820	$\pi_{\text{MIm}^-,1} \rightarrow \pi_2^*$

Table S7: Chl $a \cdots$ MIm$^-$, Franck-Condon point, SCS-ωPBEPP86/def2-TZVP. The respective orbitals are illustrated in fig. S11.

state	ΔE [eV]	osc	weight	CI transition
S$_1$	1.86	0.2635	0.736	$\pi_1 \rightarrow \pi_1^*$
S$_2$	2.00	0.0362	0.566	$\pi_2 \rightarrow \pi_1^*$
			0.315	$\pi_1 \rightarrow \pi_2^*$
S$_3$	2.05	0.0013	0.966	$\pi_{\text{MIm}^-,1} \rightarrow \pi_1^*$
S$_4$	2.94	0.0641	0.777	$\pi_{\text{MIm}^-,1} \rightarrow \pi_2^*$
S$_5$	3.04	0.8719	0.226	$\pi_2 \rightarrow \pi_1^*$
			0.498	$\pi_1 \rightarrow \pi_2^*$
S$_6$	3.10	0.8911	0.569	$\pi_2 \rightarrow \pi_2^*$
S$_7$	3.31	0.7360	0.433	$\pi_4 \rightarrow \pi_1^*$
S$_8$	3.33	0.0230	0.353	$\pi_5 \rightarrow \pi_1^*$

Table S8: Chl $a\cdots\text{MIm}^-$, S_1 minimum, DFT/MRCI. The respective orbitals are illustrated in fig. S11.

state	ΔE [eV]	osc	CI weight	CI transition
S_1	0.53	0.0001	0.887	$\pi_{\text{MIm}^-,1} \to \pi_1^*$
S_2	1.58	0.0003	0.820	$\pi_{\text{MIm}^-,1} \to \pi_2^*$
S_3	1.95	0.4446	0.745	$\pi_1 \to \pi_1^*$
S_4	2.05	0.1285	0.711	$\pi_2 \to \pi_1^*$

Table S9: Chl $a\cdots\text{MIm}^-$, S_1 minimum, SCS-ωPBEPP86/def2-TZVP. The respective orbitals are illustrated in fig. S11.

state	ΔE [eV]	osc	CI weight	CI transition
S_1	0.66	0.0001	0.993	$\pi_{\text{MIm}^-,1} \to \pi_1^*$
S_2	1.83	0.0013	0.985	$\pi_{\text{MIm}^-,1} \to \pi_2^*$
S_3	1.84	0.3467	0.765	$\pi_1 \to \pi_1^*$
S_4	1.92	0.1197	0.693	$\pi_2 \to \pi_1^*$
S_5	2.85	0.1368	0.745	$\pi_{\text{MIm}^-,2} \to \pi_1^*$
S_6	2.96	0.0391	0.721	$\pi_4 \to \pi_1^*$
S_7	3.11	0.8397	0.532	$\pi_1 \to \pi_2^*$
S_8	3.15	0.4137	0.463	$\pi_5 \to \pi_1^*$

Figure S11: MOs with labels as in tables S6 to S9. The π-orbtials located on the chlorophyll molecule are numbered according to fig. S10 (Isovalue: 0.02).

5.3 Chlorophyll $a \cdots$ MImH assembly

Table S10: Chl $a \cdots$ MImH, DFT/MRCI. The respective orbitals are illustrated in fig. S12.

state	ΔE [eV]	osc	CI weight	CI transition
S_1	1.98	0.3380	0.719	$\pi_1 \to \pi_1^*$
S_2	2.18	0.0514	0.622	$\pi_2 \to \pi_1^*$
S_3	3.09	0.6190	0.480	$\pi_1 \to \pi_2^*$
S_4	3.14	0.3698	0.508	$\pi_4 \to \pi_1^*$

Table S11: Chl $a \cdots$ MImH, SCS-ωPBEPP86/def2-TZVP. The respective orbitals are illustrated in fig. S12.

state	ΔE [eV]	osc	CI weight	CI transition
S_1	1.88	0.2612	0.745	$\pi_1 \to \pi_1^*$
S_2	2.08	0.0386	0.563	$\pi_2 \to \pi_1^*$
			0.339	$\pi_1 \to \pi_2^*$
S_3	3.15	0.5842	0.327	$\pi_1 \to \pi_2^*$
			0.265	$\pi_4 \to \pi_1^*$
S_4	3.24	1.1210	0.608	$\pi_2 \to \pi_2^*$
S_5	3.32	0.9864	0.221	$\pi_1 \to \pi_2^*$
			0.363	$\pi_4 \to \pi_1^*$
S_6	3.32	0.0459	0.548	$\pi_5 \to \pi_1^*$
S_7	3.64	0.2943	0.595	$\pi_6 \to \pi_1^*$
S_8	3.67	0.0022	0.289	$LP_O \to \pi_3^*$
			0.297	$LP_O \to \pi_1^*$

5.4 Chlorophyll $a \cdots$ MImH$_2^+$ assembly

Table S12: Chl $a \cdots$ MImH$_2^+$, DFT/MRCI. The respective orbitals are illustrated in fig. S12.

state	ΔE [eV]	osc	CI weight	CI transition
S_1	2.04	0.3546	0.757	$\pi_1 \to \pi_1^*$
S_2	2.29	0.0276	0.548	$\pi_2 \to \pi_1^*$
			0.260	$\pi_1 \to \pi_2^*$
S_3	2.99	0.0370	0.713	$\pi_4 \to \pi_1^*$
S_4	3.18	0.5882	0.323	$\pi_1 \to \pi_2^*$
			0.176	$\pi_5 \to \pi_1^*$

Table S13: Chl $a \cdots$ MImH$_2^+$, SCS-ωPBEPP86/def2-TZVP. The respective orbitals are illustrated in fig. S12.

state	ΔE [eV]	osc	CI weight	CI transition
S_1	1.89	0.2704	0.790	$\pi_1 \to \pi_1^*$
S_2	2.15	0.0160	0.515	$\pi_2 \to \pi_1^*$
			0.416	$\pi_1 \to \pi_2^*$
S_3	3.12	0.0956	0.725	$\pi_4 \to \pi_1^*$
S_4	3.19	1.3081	0.367	$\pi_2 \to \pi_1^*$
			0.452	$\pi_1 \to \pi_2^*$
S_5	3.25	0.0516	0.675	$\pi_5 \to \pi_1^*$
S_6	3.38	1.2031	0.646	$\pi_2 \to \pi_2^*$
S_7	3.52	0.0086	0.241	$LP_O \to \pi_1^*$
			0.257	$LP_O \to \pi_3^*$
S_8	3.55	0.2761	0.654	$\pi_6 \to \pi_1^*$

π_1^* π_2^* π_3^*

π_1 π_2 π_4 π_5 π_6 LP_O
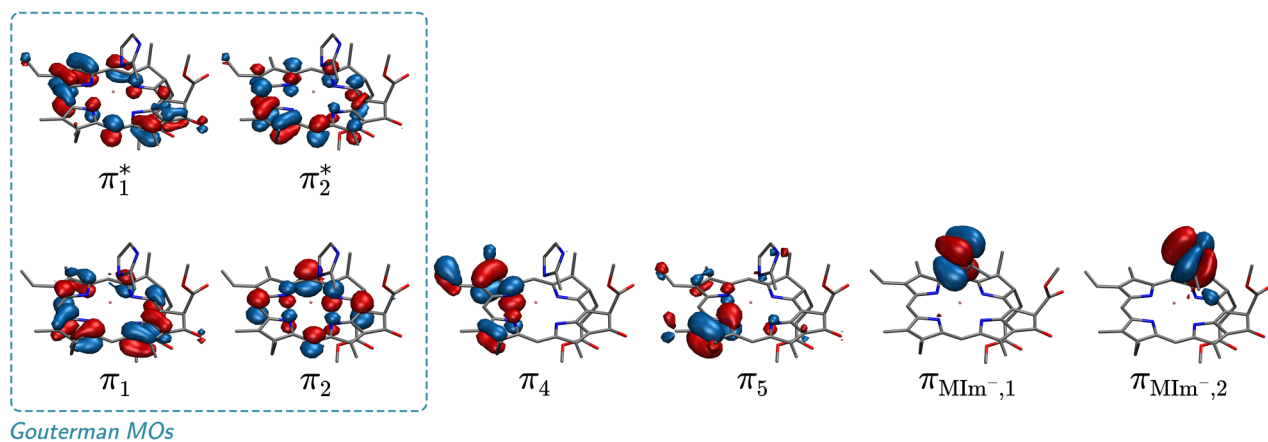
Gouterman MOs
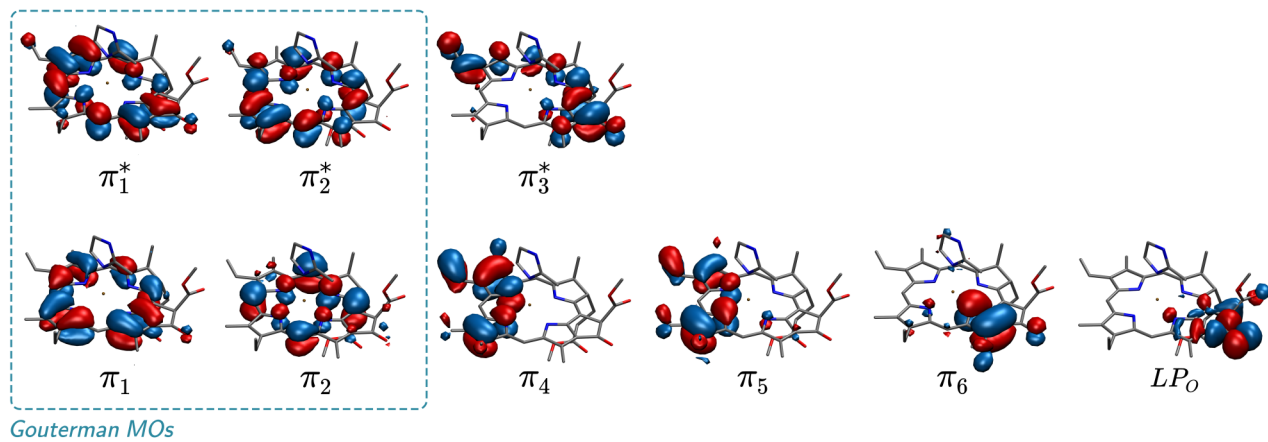
Figure S12: MOs with labels as in tables S10 to S13. The π-orbtials located on the chlorophyll molecule are numbered according to fig. S10 (Isovalue: 0.02).

6 Statistics of QM/MM Sampling

Table S14: Mean and standard deviation σ among the three types of coordination in the sampled data points.

<table>
<tr><td colspan="4" align="center">(a) CT number</td><td colspan="4" align="center">(b) Energies</td></tr>
<tr><td>coord.</td><td>samples</td><td>$\overline{\text{CT}}$</td><td>σ</td><td>coord.</td><td>samples</td><td>$\Delta\overline{\text{E}}$ [eV]</td><td>σ [eV]</td></tr>
<tr><td>0</td><td>51</td><td>0.000</td><td>0.000</td><td>0</td><td>51</td><td>1.898</td><td>0.054</td></tr>
<tr><td>1</td><td>93</td><td>0.809</td><td>0.279</td><td>1</td><td>93</td><td>1.434</td><td>0.320</td></tr>
<tr><td>2</td><td>11</td><td>0.893</td><td>0.102</td><td>2</td><td>11</td><td>1.198</td><td>0.563</td></tr>
</table>

7 Excitons in the Presence of ZIF-8

7.1 Comparison with Free PS I
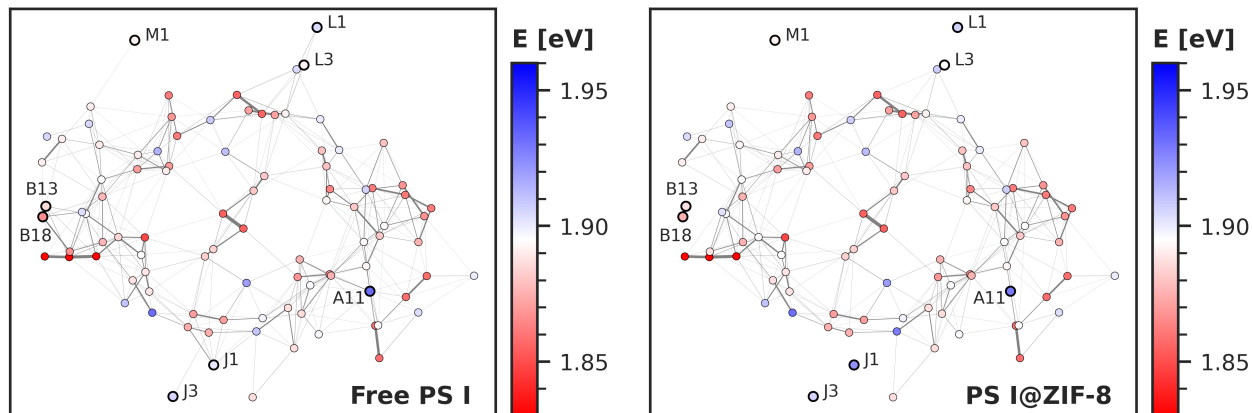
Figure S13: Left: Unperturbed excitonic network in PS I.[S3] Right: The same network when the highlighted, frequently coordinated chlorophylls are not coupled. Each data point represents one chlorophyll, colored by the lowest-energy exciton it contributes to. Thicker lines signify stronger excitonic coupling. View from the stromal side.

7.2 List of Excitonic Energies and Pigment Contributions

Table S15: Exciton energies and chlorophyll contributions to each exciton. Chlorophylls are assigned to an exciton domain if their weight w_i in the excitonic wavefunction is larger than 0.1. Contribution coefficients c_i of each chlorophyll to the respective exciton are also provided. Table rows are sorted in ascending order by the exciton energy E_{exc}. The column *ID (MD)* refers to the residue ID used in our MD simulations, while *Name* denotes the standard residue numbering scheme in PS I[S16,S17] and *ID (x-ray)* is the residue ID used in the crystal structure PDB (1JB0).[S16]

| Exciton	E_{exc} [eV]	name	ID (MD)	ID (x-ray)	w_i	c_i
0	1.828088	B31	2416	1231	0.195925	0.442634
	1.828088	B32	2417	1232	0.648848	-0.805511
	1.828088	B33	2418	1233	0.153045	0.391210
1	1.848102	B22	2407	1222	0.932374	-0.965595
2	1.854704	eC-A1	2337	1011	0.509149	0.713547
	1.854704	eC-B1	2383	1021	0.390128	-0.624602
3	1.855147	B7	2392	1207	0.650815	-0.806731
	1.855147	A32	2371	1132	0.309593	0.556411
4	1.857635	A10	2349	1110	0.799544	0.894172
	1.857635	A18	2357	1118	0.140763	-0.375183
5	1.858305	A12	2351	1112	0.528240	-0.726801
	1.858305	A14	2353	1114	0.443728	0.666129
6	1.861035	A34	2373	1134	0.505303	0.710847
	1.861035	A33	2372	1133	0.147228	-0.383703
	1.861035	K1	2427	1401	0.244595	-0.494566
7	1.861079	B4	2389	1204	0.101061	-0.317902
	1.861079	B5	2390	1205	0.718982	0.847928
8	1.863935	A35	2374	1135	0.760835	0.872259
9	1.867531	A21	2360	1121	0.178762	-0.422803
	1.867531	A20	2359	1120	0.778031	0.882061
10	1.868089	A26	2365	1126	0.333405	-0.577412
	1.868089	A27	2366	1127	0.612573	0.782670
11	1.868464	B1	2386	1201	0.877538	0.936770
12	1.870032	B25	2410	1225	0.178489	-0.422479
	1.870032	B24	2409	1224	0.661842	0.813537
13	1.870611	A38	2377	1138	0.366831	-0.605665
	1.870611	A39	2378	1139	0.581475	0.762545
14	1.871598	B38	2422	1238	0.596097	0.772073
	1.871598	B37	2380	1237	0.357361	-0.597797
15	1.874772	B30	2415	1230	0.777110	0.881539
	1.874772	B29	2414	1229	0.146486	-0.382734
16	1.875467	A15	2354	1115	0.557350	0.746559
	1.875467	K1	2427	1401	0.178492	-0.422483
17	1.875521	B21	2406	1221	0.678866	-0.823933
	1.875521	B20	2405	1220	0.227798	0.477282

continued on next page

Table S15: continued.

Exciton	E_{exc} [eV]	name	ID (MD)	ID (x-ray)	w_i	c_i
18	1.875533	B18	2403	1218	1.000000	1.000000
19	1.875636	A28	2367	1128	0.279299	-0.528487
	1.875636	A3	2342	1103	0.525045	0.724600
20	1.879495	A37	2376	1137	0.184435	-0.429459
	1.879495	PL1	2382	1801	0.306897	-0.553983
	1.879495	A36	2375	1136	0.160531	0.400664
21	1.880347	PL1	2382	1801	0.579592	-0.761309
22	1.881054	eC-A2	2338	1022	0.356157	-0.596789
	1.881054	A16	2355	1116	0.128110	-0.357925
	1.881054	eC-B3	2385	1023	0.122730	0.350329
	1.881054	A25	2364	1125	0.151849	0.389678
23	1.882959	eC-B2	2384	1012	0.544657	-0.738009
	1.882959	eC-A3	2339	1013	0.161406	0.401753
24	1.884312	A16	2355	1116	0.131323	0.362385
	1.884312	eC-A2	2338	1022	0.177744	-0.421597
	1.884312	A36	2375	1136	0.158540	-0.398171
	1.884312	A37	2376	1137	0.166873	0.408501
25	1.884616	B31	2416	1231	0.388471	-0.623274
	1.884616	B33	2418	1233	0.387574	0.622554
26	1.886691	A2	2341	1102	0.139463	-0.373448
	1.886691	A6	2345	1106	0.319840	-0.565544
	1.886691	A28	2367	1128	0.153778	0.392146
	1.886691	J2	2425	1302	0.151099	-0.388715
	1.886691	A5	2344	1105	0.131068	0.362033
27	1.887096	B19	2404	1219	0.167401	-0.409147
	1.887096	B21	2406	1221	0.153884	0.392281
	1.887096	B20	2405	1220	0.175134	0.418490
	1.887096	B27	2412	1227	0.378037	-0.614847
28	1.887160	B13	2398	1213	1.000000	-1.000000
29	1.887162	A6	2345	1106	0.139227	-0.373132
	1.887162	A3	2342	1103	0.101675	-0.318865
	1.887162	A28	2367	1128	0.336348	-0.579955
	1.887162	A2	2341	1102	0.210149	0.458420
	1.887162	J2	2425	1302	0.100819	-0.317520
30	1.888162	B35	2420	1235	0.121318	0.348307
	1.888162	B4	2389	1204	0.457553	0.676426
31	1.888564	B35	2420	1235	0.275329	-0.524718
	1.888564	B4	2389	1204	0.212466	0.460940
	1.888564	B36	2421	1236	0.154960	0.393650
32	1.890059	A6	2345	1106	0.151294	0.388966
	1.890059	J2	2425	1302	0.516858	-0.718928
33	1.890118	B2	2387	1202	0.137058	0.370213
	1.890118	B26	2411	1226	0.227074	-0.476523
	1.890118	J2	2425	1302	0.183566	-0.428446

Table S15: continued.

Exciton	E_{exc} [eV]	name	ID (MD)	ID (x-ray)	w_i	c_i
34	1.890433	B19	2404	1219	0.148855	0.385817
	1.890433	B9	2394	1209	0.302101	-0.549637
	1.890433	B27	2412	1227	0.166039	-0.407478
	1.890433	B17	2402	1217	0.113012	0.336172
35	1.891271	B17	2402	1217	0.128398	-0.358327
	1.891271	B19	2404	1219	0.126846	0.356155
	1.891271	B9	2394	1209	0.345745	0.588001
	1.891271	B8	2393	1208	0.102065	-0.319476
36	1.891988	B7	2392	1207	0.110304	-0.332120
	1.891988	A31	2370	1131	0.493989	0.702843
	1.891988	A32	2371	1132	0.144535	-0.380178
37	1.892145	M1	2431	1601	1.000000	1.000000
38	1.892732	A17	2356	1117	0.267405	-0.517112
	1.892732	A24	2363	1124	0.107370	-0.327674
	1.892732	A26	2365	1126	0.226199	0.475603
39	1.893462	B26	2411	1226	0.231486	0.481130
	1.893462	B8	2393	1208	0.554302	0.744514
	1.893462	B10	2395	1210	0.129429	-0.359762
40	1.894031	A21	2360	1121	0.109612	0.331077
	1.894031	A19	2358	1119	0.637051	-0.798155
	1.894031	A23	2362	1123	0.147290	0.383784
41	1.894138	L3	2430	1503	1.000000	1.000000
42	1.894143	A8	2347	1108	0.877256	0.936620
43	1.894917	B23	2408	1223	0.136893	0.369990
	1.894917	B34	2419	1234	0.119035	-0.345014
	1.894917	B14	2399	1214	0.291036	-0.539477
	1.894917	B15	2400	1215	0.188578	0.434255
44	1.896232	A4	2343	1104	0.268393	-0.518066
	1.896232	A3	2342	1103	0.130076	0.360661
	1.896232	A9	2348	1109	0.106773	-0.326761
	1.896232	A2	2341	1102	0.323645	0.568898
45	1.897242	A27	2366	1127	0.153255	-0.391478
	1.897242	A26	2365	1126	0.249767	-0.499767
	1.897242	A33	2372	1133	0.190662	-0.436649
46	1.898239	B10	2395	1210	0.126105	0.355113
	1.898239	A38	2377	1138	0.130784	0.361641
	1.898239	A1	2340	1101	0.226349	-0.475761
47	1.898412	B10	2395	1210	0.193242	-0.439593
	1.898412	A38	2377	1138	0.165018	0.406224
	1.898412	A1	2340	1101	0.299346	-0.547125
49	1.898832	A24	2363	1124	0.114051	-0.337714
	1.898832	A33	2372	1133	0.100149	0.316463
50	1.899573	A29	2368	1129	0.231297	-0.480934
	1.899573	A30	2369	1130	0.463129	0.680536
	1.899573	K2	2381	1402	0.115358	-0.339644
51	1.899858	K2	2381	1402	0.719781	-0.848399

Table S15: continued.

Exciton	E_{exc} [eV]	name	ID (MD)	ID (x-ray)	w_i	c_i
52	1.902253	B19	2404	1219	0.233577	-0.483298
	1.902253	B20	2405	1220	0.360797	-0.600664
	1.902253	B16	2401	1216	0.149756	0.386983
53	1.903326	B29	2414	1229	0.572155	-0.756410
54	1.903526	A13	2352	1113	0.835026	-0.913798
55	1.904648	B12	2397	1212	0.170047	-0.412368
	1.904648	A17	2356	1117	0.143394	0.378674
56	1.904701	A17	2356	1117	0.112090	0.334798
	1.904701	B12	2397	1212	0.263689	0.513506
	1.904701	B25	2410	1225	0.112739	0.335766
57	1.905588	B12	2397	1212	0.438807	-0.662425
	1.905588	B25	2410	1225	0.207668	0.455706
58	1.905978	J3	2426	1303	1.000000	1.000000
59	1.906370	L1	2428	1501	1.000000	-1.000000
60	1.906722	A9	2348	1109	0.238936	0.488811
	1.906722	A22	2361	1122	0.113133	0.336352
	1.906722	A23	2362	1123	0.439689	-0.663090
61	1.907346	A4	2343	1104	0.212051	0.460490
	1.907346	A5	2344	1105	0.107615	-0.328047
	1.907346	A9	2348	1109	0.410185	-0.640457
62	1.907592	L2	2429	1502	0.524420	0.724168
	1.907592	B6	2391	1206	0.143100	0.378286
63	1.909004	A38	2377	1138	0.208253	0.456347
	1.909004	A39	2378	1139	0.216828	0.465648
	1.909004	A1	2340	1101	0.240844	0.490758
64	1.909493	L2	2429	1502	0.138602	0.372293
	1.909493	A5	2344	1105	0.198904	0.445986
65	1.909616	A5	2344	1105	0.213995	-0.462596
	1.909616	L2	2429	1502	0.187462	0.432969
	1.909616	B6	2391	1206	0.128049	-0.357839
66	1.910026	X1	2432	1701	0.195606	-0.442274
	1.910026	B35	2420	1235	0.151312	0.388988
	1.910026	B11	2396	1211	0.118044	-0.343576
67	1.911992	B39	2423	1239	0.399060	-0.631712
	1.911992	B6	2391	1206	0.105547	-0.324880
	1.911992	B2	2387	1202	0.130006	0.360563
68	1.912639	B11	2396	1211	0.315743	-0.561910
	1.912639	B39	2423	1239	0.161665	0.402075
	1.912639	B2	2387	1202	0.108282	0.329062
69	1.914304	B11	2396	1211	0.158450	0.398058
	1.914304	B10	2395	1210	0.104274	0.322915
	1.914304	B3	2388	1203	0.128770	-0.358845
	1.914304	B2	2387	1202	0.211201	0.459566

Table S15: continued.

Exciton	E_{exc} [eV]	name	ID (MD)	ID (x-ray)	w_i	c_i
70	1.915613	A20	2359	1120	0.103825	0.322219
	1.915613	A21	2360	1121	0.339017	0.582251
	1.915613	A23	2362	1123	0.118541	-0.344298
	1.915613	A22	2361	1122	0.271081	-0.520654
71	1.916176	A18	2357	1118	0.255012	0.504988
	1.916176	A34	2373	1134	0.104146	-0.322717
72	1.917261	A18	2357	1118	0.412792	0.642489
73	1.918720	B37	2380	1237	0.357297	0.597744
	1.918720	B38	2422	1238	0.225130	0.474479
74	1.919671	B16	2401	1216	0.399464	0.632032
75	1.919936	B16	2401	1216	0.118781	-0.344646
	1.919936	eC-A3	2339	1013	0.233494	-0.483212
	1.919936	A40	2379	1140	0.228207	0.477710
76	1.921194	A37	2376	1137	0.135833	0.368555
77	1.922410	A4	2343	1104	0.114748	0.338745
78	1.922465	J1	2424	1301	1.000000	-1.000000
79	1.923637	X1	2432	1701	0.223642	-0.472908
	1.923637	B34	2419	1234	0.192104	0.438297
	1.923637	B23	2408	1223	0.143297	0.378547
80	1.924516	A12	2351	1112	0.197625	-0.444551
	1.924516	A14	2353	1114	0.216729	-0.465541
81	1.924983	B33	2418	1233	0.175255	-0.418635
	1.924983	B31	2416	1231	0.132504	-0.364011
	1.924983	B15	2400	1215	0.169140	0.411267
	1.924983	B32	2417	1232	0.166779	-0.408386
82	1.926521	A29	2368	1129	0.133007	0.364702
	1.926521	eC-B3	2385	1023	0.335708	-0.579403
	1.926521	B39	2423	1239	0.120227	-0.346737
83	1.928397	A7	2346	1107	0.180694	-0.425081
	1.928397	A40	2379	1140	0.287016	0.535739
84	1.928800	A11	2350	1111	1.000000	1.000000
85	1.928964	eC-B3	2385	1023	0.112963	-0.336100
	1.928964	A40	2379	1140	0.149283	-0.386371
	1.928964	A32	2371	1132	0.104614	0.323441
86	1.932066	X1	2432	1701	0.130374	0.361074
	1.932066	B28	2413	1228	0.241287	-0.491210
	1.932066	B36	2421	1236	0.173693	0.416765
87	1.933187	A6	2345	1106	0.127127	-0.356549
	1.933187	A7	2346	1107	0.338049	-0.581420
88	1.934316	B3	2388	1203	0.360470	0.600392
	1.934316	B17	2402	1217	0.176799	-0.420474
89	1.936331	A32	2371	1132	0.107432	-0.327767
	1.936331	B17	2402	1217	0.140836	0.375281
	1.936331	A22	2361	1122	0.173899	0.417012
90	1.937941	B17	2402	1217	0.210714	-0.459036

continued on next page

Table S15: continued.

Exciton	E_{exc} [eV]	name	ID (MD)	ID (x-ray)	w_i	c_i
91	1.939294	B17	2402	1217	0.132350	-0.363800
	1.939294	B3	2388	1203	0.139629	-0.373670
92	1.939766	B27	2412	1227	0.117600	0.342929
	1.939766	B28	2413	1228	0.447904	0.669256
93	1.947151	A22	2361	1122	0.109347	-0.330676
94	1.954365	eC-A1	2337	1011	0.233655	0.483379
	1.954365	eC-B1	2383	1021	0.296717	0.544717
95	1.962355	B31	2416	1231	0.130906	-0.361810
	1.962355	B23	2408	1223	0.273667	-0.523132

References

(S1) Balestra, S. R. G.; Semino, R. Computer Simulation of the Early Stages of Self-Assembly and Thermal Decomposition of ZIF-8. *J. Chem. Phys.* **2022**, *157*, 184502.

(S2) Balestra, S. R. G. Codes and supporting data for Computer Simulation of the Early and Late Stages of the Self-Assembly of ZIF-8. 2022; https://github.com/salrodgom/ZIFWTMetaDnbZIFFF, (accessed 11 July 2024).

(S3) Reiter, S.; Kiss, F. L.; Hauer, J.; de Vivie-Riedle, R. Thermal Site Energy Fluctuations in Photosystem I: New Insights from MD/QM/MM Calculations. *Chem. Sci.* **2023**, *14*, 3117–3131.

(S4) Hess, B.; Bekker, H.; Berendsen, H. J. C.; Fraaije, J. G. E. M. LINCS: A Linear Constraint Solver for Molecular Simulations. *J. Comput. Chem.* **1997**, *18*, 1463–1472.

(S5) Páll, S.; Hess, B. A Flexible Algorithm for Calculating Pair Interactions on SIMD Architectures. *Comput. Phys. Commun.* **2013**, *184*, 2641–2650.

(S6) Darden, T.; York, D.; Pedersen, L. Particle Mesh Ewald: An N·log(N) Method for Ewald Sums in Large Systems. *J. Chem. Phys.* **1993**, *98*, 10089.

(S7) Essmann, U.; Perera, L.; Berkowitz, M. L.; Darden, T.; Lee, H.; Pedersen, L. G. A Smooth Particle Mesh Ewald Method. *J. Chem. Phys.* **1995**, *103*, 8577–8593.

(S8) Eggimann, B. L.; Sunnarborg, A. J.; Stern, H. D.; Bliss, A. P.; Siepmann, J. I. An Online Parameter and Property Database for the TraPPE Force Field. *Mol. Simul.* **2014**, *40*, 101–105.

(S9) Bussi, G.; Donadio, D.; Parrinello, M. Canonical Sampling through Velocity Rescaling. *J. Chem. Phys.* **2007**, *126*, 014101.

(S10) Berendsen, H. J. C.; Postma, J. P. M.; van Gunsteren, W. F.; DiNola, A.; Haak, J. R. Molecular Dynamics with Coupling to an External Bath. *J. Chem. Phys.* **1984**, *81*, 3684–3690.

(S11) Taravillo, M.; Pérez, F. J.; Núñez, J.; Cáceres, M.; Baonza, V. G. Thermodynamic Properties of Compressed Liquid Methanol in the Vicinity of the Freezing Line. *J. Chem. Eng. Data* **2007**, *52*, 481–486.

(S12) Brostow, W.; Grindley, T.; Macip, M. A. Volumetric Properties of Organic Liquids as a Function of Temperature and Pressure: Experimental Data and Prediction of Compressibility. *Mater. Chem. Phys.* **1985**, *12*, 37–97.

(S13) Cao, S.; Bennett, T. D.; Keen, D. A.; Goodwin, A. L.; Cheetham, A. K. Amorphization of the Prototypical Zeolitic Imidazolate Framework ZIF-8 by Ball-Milling. *Chem. Commun.* **2012**, *48*, 7805–7807.

(S14) Wang, J.; Wang, W.; Kollman, P. A.; Case, D. A. Automatic Atom Type and Bond Type Perception in Molecular Mechanical Calculations. *J. Mol. Graphics* **2006**, *25*, 247–260.

(S15) Wang, J.; Wolf, R. M.; Caldwell, J. W.; Kollman, P. A.; Case, D. A. Development and Testing of a General Amber Force Field. *J. Comput. Chem.* **2004**, *25*, 1157–1174.

(S16) Jordan, P.; Fromme, P.; Witt, H. T.; Klukas, O.; Saenger, W.; Krauß, N. Three-Dimensional Structure of Cyanobacterial Photosystem I at 2.5 Å Resolution. *Nature* **2001**, *411*, 909–917.

(S17) Byrdin, M.; Jordan, P.; Krauss, N.; Fromme, P.; Stehlik, D.; Schlodder, E. Light Harvesting in Photosystem I: Modeling Based on the 2.5-Å Structure of Photosystem I from Synechococcus Elongatus. *Biophys. J.* **2002**, *83*, 433–457.